

Check for updates

www.advmattechnol.de

Engineering Anisotropic Cell Models: Development of Collagen Hydrogel Scaffolds with Magneto-Responsive PEG Microgels for Tissue Engineering Applications

Ana L. Castro, Sitara Vedaraman, Tamás Haraszti, Mário A. Barbosa, Raquel M. Gonçalves, and Laura De Laporte*

Mimicking tissue-oriented organization in vitro has been extensively studied in recent years, using both natural and synthetic materials in combination with external magnetic fields to establish anisotropic conditions. Here, a new combination between magneto-responsive anisometric PEG microgels and collagen hydrogels is explored to establish anisotropic in vitro models. Different sizes of PEG microgels are tested to assess the impact of both width and aspect ratio on the formation and alignment of collagen hydrogels. Results show that the key properties of collagen hydrogels, regarding fibrillogenesis, rheological properties, and fiber diameter are kept consistent upon the combination with PEG microgels. Furthermore, partial collagen fiber alignment is observed when larger (width 10 μm) PEG microgels are employed and magnetically aligned. In vitro studies show cell alignment within the anisotropic collagen hydrogels from the first day in culture. Interestingly, PEG microgels with higher width and length tend to induce less hydrogel contraction even after 7 days in culture. The results demonstrate the ability to establish a 3D unidirectional collagen hydrogel by magnetically aligning anisometric microgels during the gelation process, which can be promising for different tissue engineering applications.

1. Introduction

Collagen type I (Col I) is the major organic component of the extracellular matrix (ECM) of mammalian tissue.[1] Together with other ECM molecules, this protein has an important structural action for growth and support of cells, playing a relevant role in different physiological processes.[1-3] Col I acts as an attractive protein for tissue engineering both due its biocompatibility, biodegradability, and antigenicity, but also due to its ability to self-assemble and generate hydrogels.^[2-5] Indeed, Col I hydrogels have been broadly used for different applications in tissue engineering, either alone or in combination with other ECM proteins/constituents and biomaterials, as they show great results as support for 3D cell culture.[6-8]

In recent years, in vitro models have focused on providing a microenvironment

A. L. Castro, M. A. Barbosa, R. M. Gonçalves i3S – Instituto de Investigação e Inovação em Saúde Universidade do Porto 4200-135 Porto, Portugal A. L. Castro, M. A. Barbosa, R. M. Gonçalves INEB – Instituto de Engenharia Biomédica Universidade do Porto 4200-135 Porto, Portugal

The ORCID identification number(s) for the author(s) of this article can be found under https://doi.org/10.1002/admt.202301391

© 2024 The Authors. Advanced Materials Technologies published by Wiley-VCH GmbH. This is an open access article under the terms of the Creative Commons Attribution-NonCommercial-NoDerivs License, which permits use and distribution in any medium, provided the original work is properly cited, the use is non-commercial and no modifications or adaptations are made.

DOI: 10.1002/admt.202301391

A. L. Castro, M. A. Barbosa, R. M. Gonçalves ICBAS – Instituto de Ciências Biomédicas Abel Salazar Universidade do Porto 4050-313 Porto, Portugal S. Vedaraman, T. Haraszti, L. De Laporte Department of Advanced Materials for Biomedicine Institute of Applied Medical Engineering

Institute of Applied Medical Engineering RWTH Aachen University 52074 Aachen, Germany S. Vedaraman, T. Haraszti, L. De Laporte

S. Vedaraman, T. Haraszti, L. De Laporte Institute of Technical and Macromolecular Chemistry RWTH Aachen University 52074 Aachen, Germany

L. De Laporte DWI – Leibniz Institute for Interactive Materials 52074 Aachen, Germany E-mail: delaporte@dwi.rwth-aachen.de www.advancedsciencenews.com



www.advmattechnol.de

to support cell growth that beside having a 3D structure, also mimic features of the in vivo architecture. [9] Each tissue has a specific architecture, particularly regarding Col I anisotropy. Tissues, such as tendon, intervertebral disc, muscle, and others, present a specific microarchitecture composed of oriented Col I fibers, which has an impact on tissue homeostasis concerning structural and cellular processes. [10]

Several strategies have been developed to recreate the natural anisotropy observed in collagenous native tissues in an in vitro environment, which have been extensively reviewed elsewhere.[9,11,12] These strategies include biomaterial processing techniques, such as extrusion, freeze-drying, electrospinning, magnetic alignment, flow-induced orientation, among others.[13-17] Electrospinning-aligned collagen nanofibers has been proposed for different applications in wound healing, bone mineralization, and nerve tissue regeneration.[18-20] Here, an additional crosslinking step is often needed to overcome the reduction of pore size due to dense packing of aligned collagen fibers, impairing cell proliferation within the scaffold.^[21] Moreover, collagen denaturation has been reported upon electro-spinning, impairing its fibrillar structure.[22] On the other hand, for several decades, extrusion techniques have been successfully used to produce aligned collagen scaffolds, due to its ease and possibility of scale up, with applications in bone and tendon regeneration, ligament replacement, and wound healing.[9,23,24] Despite the recent advances on the combination of 3D printing with extrusion, this approach still presents limitations regarding production time and cell mortality.[9]

Magnetic alignment techniques have risen interest in recent years as they can overcome some of the most common drawbacks associated with the previously mentioned strategies, including reduced fibril formation and cell infiltration. To achieve anisotropic scaffolds, magnetic nanoparticles (e.g., iron nanoparticles) have been used together with a Col I solution to accomplish fibril alignment under an external magnetic field, both for cartilage and nerve regeneration.^[25,26] Anisotropy induced by magnetic approaches has shown promising results, albeit higher amounts of iron nanoparticles might lead to cell cytotoxicity.^[27] In this context, magnetic-responsive, rod-shaped microgels have been used to overcome this drawback, using poly(ethylene glycol) (PEG) and fibrin as surrounding hydrogels. [28-30] Briefly, a hybrid hydrogel, named Anisogel, has been established where unidirectional microgel orientation is accomplished in the presence of an external magnetic field (100 millitesla) by incorporating small amounts of superparamagnetic iron oxide nanoparticles inside PEG microgels during their production.^[29] This methodology has been thoroughly characterized in prior publications, [29–30] including analysis on inter-microgel distances depending on the microgel dimensions and amount (Figure 1B), and its successful application in various surrounding hydrogels.^[28-32] The anisotropy achieved by the aligned microgels is secured upon crosslinking of the surrounding hydrogel with cells encapsulated in 3D microenvironment.

The current work aims to develop a collagen-based Anisogel (collagen-Anisogel), using Col I as the surrounding hydrogel for the oriented PEG microgels (Figure 1A). We hypothesized that the proposed construct would provide anisotropy to growing cells in 3D, while microgel orientation would influence the properties of the Col I hydrogel. Therefore, bovine Col I was combined

with PEG microgels of different size combinations (cross-section (width) and length). Collagen fiber formation, diameter, and orientation were analyzed, together with the hydrogels' mechanical properties and the behavior of human dermal fibroblasts in collagen-Anisogels.

2. Results and Discussion

2.1. Turbidimetric Profile of Non-Oriented Collagen-Anisogel Formulations

Collagen's characteristic fibril features are possible due to a mechanism of nucleation and growth. Initially, self-assembly of collagen molecules occurs by aggregation to form nuclei and later these nuclei grow into fibrils, in a process called fibrillogenesis, evaluated using turbidimetric assays. [33,34] Turbidimetric analysis was used to monitor fibrillogenesis of collagen-Anisogel formulations, without inducing magnetic orientation, to analyze the effect of the microgels' presence (Figure 2A). PEG microgels were prepared using in mold polymerization, as previously described, [31] and combined with collagen solution prior to cross-linking. The different microgels sizes and concentrations tested are described in Figure 1B. Results obtained were grouped for microgels with the same width and presented as absorption (405 nm) versus time (Figure 2A1). They showed that absorbance increased with time, indicating fibril formation in the collagen-Anisogel formulations. To study the influence of microgel dimensions and concentrations in fibrillogenesis, the time required for initiation and completion of fibrils was measured (Figure 2A2). For all the tested formulations, the turbidimetric curves observed exhibited a sigmoidal shape, separated in three different stages: initial lag-phase, growth phase, and a plateau, reached after the formation of the hydrogel in an equilibrium of absorbance values. [34,35] Importantly, no distinct polymerization kinetics were observed between the collagen control and collagen-Anisogel formulations, which suggests the absence of alterations in fibril formation and growth mechanisms upon combination with PEG-µgels, [32] with median lag times ranging widely from 20.2 to 34.2 min. Formulations with smaller widths (2.5 and 5 µm) showed an increase on final A405 values compared to the collagen control, possibly related to the higher amount of PEG microgels (calculated previously^[30]) within the formulation. In general, the absorbance spectra showed that the addition of PEG microgels, independently of their size and concentration, preserved collagen's fiber formation.

2.2. Rheological Properties of Non-Oriented Collagen-Anisogels

To investigate possible alterations in basal collagen mechanical properties by the combination with PEG-µgels, rheological studies were performed. The storage and loss modulus of the collagen-Anisogel formulations were measured upon in situ gelation at 37 $^{\circ}$ C for a period of 45 min. The storage modulus after reaching the plateau at the end of the analysis of each formulation is presented in Figure 2B, grouped for microgels with the same width. For the control group (collagen alone formulation), the storage modulus observed was 136 \pm 13 Pa. The median storage

and-conditions) on Wiley Online Library for rules of use; OA articles are governed by the applicable Creative Commons

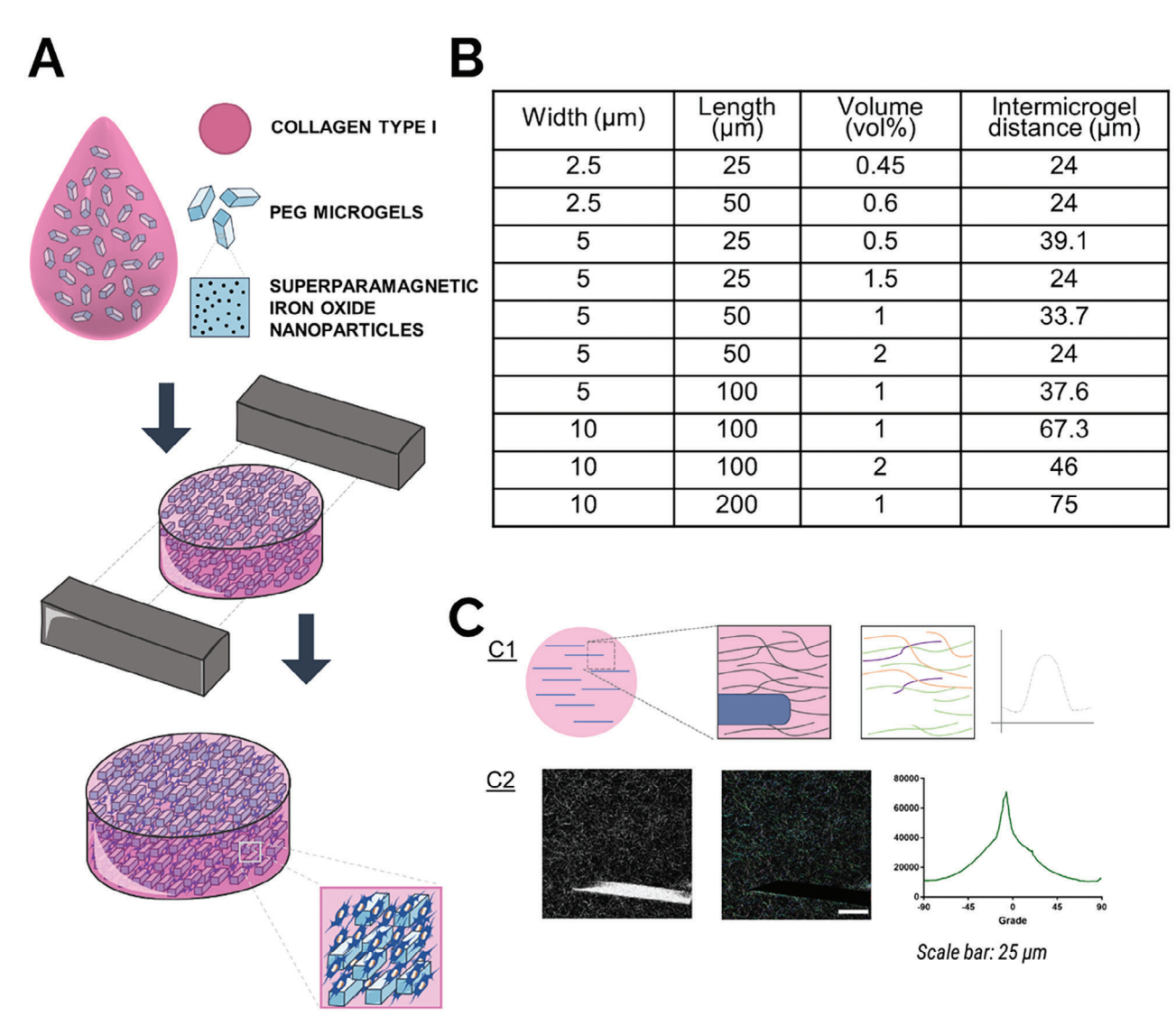


Figure 1. A) Schematic representation of the experimental setup. B) Microgel's sizes description for all formulations evaluated. C) (C1) Schematic representation of the orientation of collagen fibers surrounding the microgels, which were analyzed analysis using Orientation J. (C2) Example given with fiber orientation analysis on confocal reflection microscopy images.

modulus of the different collagen-Anisogel formulations ranged from 95 \pm 53 to 314 \pm 190 Pa, with no statistically significant difference between formulations and the control group. These data demonstrated that the addition of PEG microgels does not significantly impact the hydrogel's mechanical properties, in nonoriented conditions, as similar stiffnesses were observed among all the formulations tested. Previous work on rheological studies of PEG hydrogels upon PEG microgels incorporation have also reported similar storage moduli between the control and Anisogel groups. $^{[31]}$

2.3. Collagen Fiber Diameter Characterization in Collagen-Anisogels

As the collagen macroscopic properties were not altered with different PEG-µgel dimensions and concentrations, we probed the

microscopic alterations after magnetic microgel orientation inside collagen-Anisogels. Microgel alignment was observed along the magnetic field lines within the collagen hydrogels (Figure S1, Supporting Information). This is similar to previously reported Anisogels that were formulated with a surrounding fibrin hydrogel stabilized by Ca2+ ions^[28] or PEG hydrogel that are enzymatically crosslinked.[32] Next, we assessed the influence of aligning PEG-µgels inside the collagen solution during gelation on the collagen fiber diameters. This can be achieved using confocal reflectance microscopy (CRM) where the collagen fibers are reflected using 488 nm laser, a popular technique to visualize collagen structures.[36] A series of images of collagen control and collagen-Anisogels, both in oriented and non-oriented conditions, were captured at high magnification for fiber visualization (Figure 3). As PEG-µgels were also reflected, as observed in Figure 3, before proceeding to diameter and orientation evaluation, all images were corrected

elibrary.wiley.com/doi/10.1002/admt.202301391 by Rwth Aachen Hochschulbibliothek, Wiley Online Library on [02/08/2024]. See the Terms

ns) on Wiley Online Library for rules of use; OA articles are governed by the applicable Creative Commons



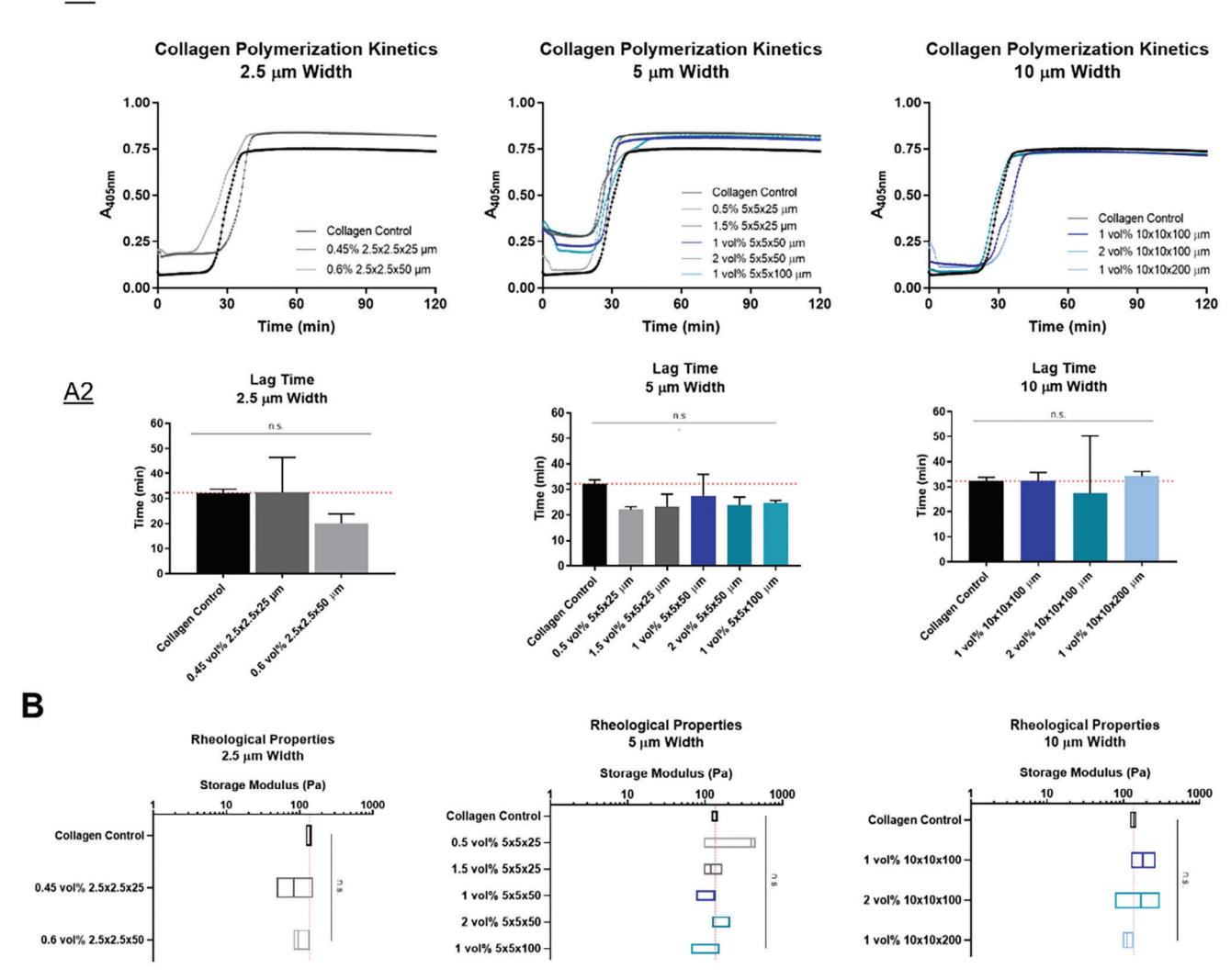


Figure 2. Collagen-Anisogels formulations characterization in non-oriented conditions. A) Fibrillogenesis analysis of collagen-Anisogels formulations: A1) Polymerization Kinetics profiles; A2) Lag Time evaluation for different formulations. Data presented using bar graphs, with median and interquartile range. B) Rheological properties of collagen-anisogels. Data presented using box plot. with median and interquartile range.

in Fiji software to remove the artifacts caused by the PEG microgels.

Fibers' diameters were analyzed to evaluate alterations in the presence of oriented PEG-µgels. A script was designed to evaluate the thickness of the fibers using python. Diameters were calculated by measuring the pixels from the CRM images and grouped considering diameter ranges of 0–400, 400–800, 800–1200, and 1200 nm and above. **Figure 4**A shows the representation of the collagen control and all collagen-Anisogels tested, grouped again by microgel width.

Starting with the 2.5 μ m wide microgels, no differences were observed between the collagen control and collagen-Anisogels for the smallest fiber diameters. When looking into diameters ranging from 400 to 800 nm, we observed a significant decrease in the fiber diameter in 0.6 vol.% 2.5 \times 2.5 \times 50 μ m microgels condition. Interestingly, this condition showed a

tendency for enabling fibrils with larger diameter fibers (>1200 nm).

Looking into the 5 μm wide microgels, for the longer length (5 \times 5 \times 100 μm microgel condition), we observed a similar trend compared to the collagen control for all diameter ranges. For the other tested conditions within this group, a tendency for higher frequency in smaller diameters (<400 nm) and a decreased frequency in intermediate diameters (400 to 800 nm) was observed, when compared with collagen control. However, statistically significant differences were only observed for 1.5 vol.% $5 \times 5 \times 25 \ \mu m$ microgels condition. For the larger fiber diameters (>800 nm), no differences were observed between the collagen control and collagen-Anisogels.

Regarding the 10 μm wide microgels, the 1 vol.% $10 \times 10 \times 200 \ \mu m$ microgels condition showed significant alterations in fiber diameter, compared to the collagen control,

ions) on Wiley Online Library for rules of use; OA articles are governed by the applicable Creative Commons

COLLAGEN

0.45 vol% 2.5x2.5x25

ξ

0.6 vol% 2.5x2.5x50

ξ

10x10x100

Wol%

Ę

10x10x100

2 vol%

10x10x200

10 µ M WIDTH

2.5 µM WIDTH

BRIGHTFIELD

ORIENTED

CRM

ORIENTED

Not Applicable CRM

NOT ORIENTED

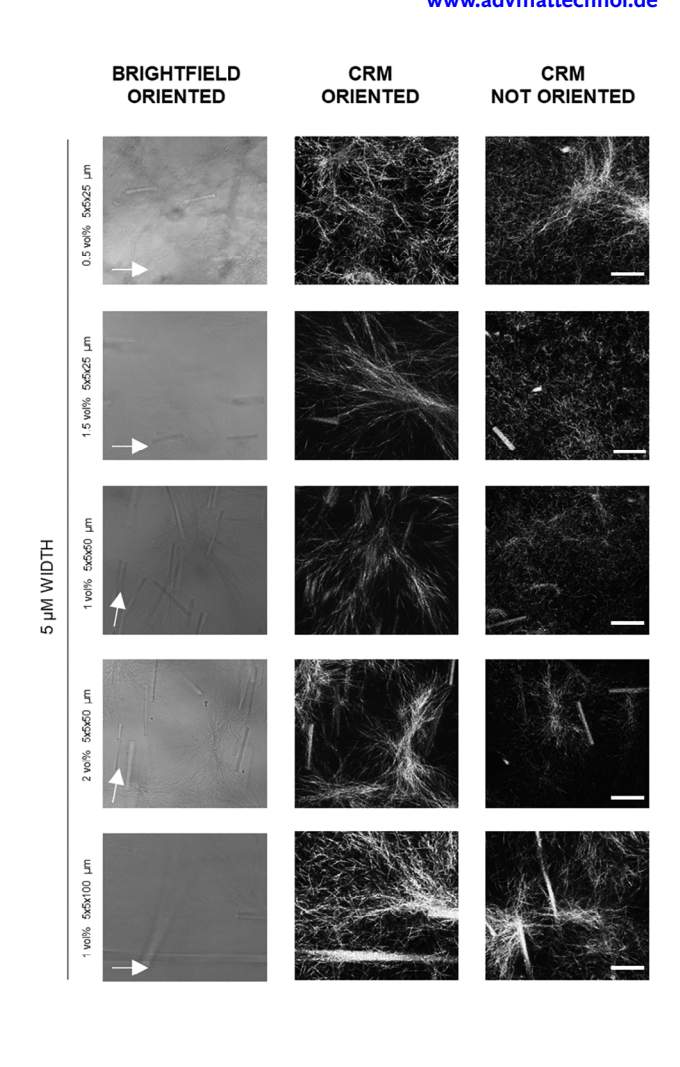


Figure 3. Fiber characterization in collagen-Anisogels. Representative brightfield and confocal reflectance microscopy images for collagen control and tested conditions of collagen-Anisogel both with and without magnetic stimuli. White arrows indicate the direction of the magnetic field and PEG microgels. Scale bar: 25 μm.

namely with an increase in <400 nm diameter and decrease in 400-800 nm. The other two conditions, both with a length of 100 µm, showed structures similar to collagen control for all the fiber diameters analyzed. Overall, by comparing with collagen control, the significant alterations mainly involved an increase in thinner fibers (diameter <400 nm) accompanied by a decrease in middle size diameter (diameter between 400 and 800 nm), as seen in 1.5 vol.% $5 \times 5 \times 25 \mu m$ and 1 vol.% $10 \times 10 \times 200 \mu m$ microgels conditions. For 0.6 vol.% $2.5 \times 2.5 \times 50 \,\mu m$ microgels condition, a decrease on middle size diameter and a tendency for an increase of larger fibers (diameter >1200 nm) was observed. Previous studies using combinations of collagen and other biomaterials have shown alterations in fiber diameter. For instance, when combining a high chondroitin sulfate concentration with collagen, increase or decrease in fiber bundling has been reported.[37] The impact of fiber diameter on cell morphology

has been analyzed as well in previous studies. For example, in poly Lactic-co-Glycolic Acid (PLGA) meshes cultured with NIH3T3 fibroblasts, an increased fiber diameter (>1400 nm) was shown to enhance aspect ratios and projected cell areas, while cells cultured in meshes with smaller fiber diameters (<400 nm) exhibited reduced cell spreading.[38] Additionally, the impact of fiber diameter on human dermal fibroblasts has been assessed in electrospun bioresorbable poly(desamino tyrosyl-tyrosine ethyl ester carbonate) scaffolds, showing that smaller fiber diameters (≈600 nm) exhibited less focal adhesion complexes compared to larger diameters (>2000 nm). The increased diameters also allowed for higher long-term (above 2 weeks) cell proliferation.^[39] As most of the tested collagen-Anisogels retained the diameter profile similar to the collagen control, the addition of PEG microgels is likely to not affect the collagen hydrogel function during 3D cell culture.

2365709x, 2024, 8, Downloaded from https://onlinelibrary.wiley.com/doi/10.1002/admt.202301391 by Rwth Aachen Hochschulbibliothek, Wiley Online Library on [02.08.2024]. See the Terms and Conditions (https://onlinelibrary.wiley.com/doi/10.1002/admt.202301391 by Rwth Aachen Hochschulbibliothek, Wiley Online Library on [02.08.2024]. See the Terms and Conditions (https://onlinelibrary.wiley.com/doi/10.1002/admt.202301391 by Rwth Aachen Hochschulbibliothek, Wiley Online Library on [02.08.2024]. See the Terms and Conditions (https://onlinelibrary.wiley.com/doi/10.1002/admt.202301391 by Rwth Aachen Hochschulbibliothek, Wiley Online Library on [02.08.2024]. See the Terms and Conditions (https://onlinelibrary.wiley.com/doi/10.1002/admt.202301391 by Rwth Aachen Hochschulbibliothek, Wiley Online Library on [02.08.2024]. See the Terms and Conditions (https://onlinelibrary.wiley.com/doi/10.1002/admt.202301391 by Rwth Aachen Hochschulbibliothek, Wiley Online Library.

and-conditions) on Wiley Online Library for rules of use; OA articles are governed by the applicable Creative Commons

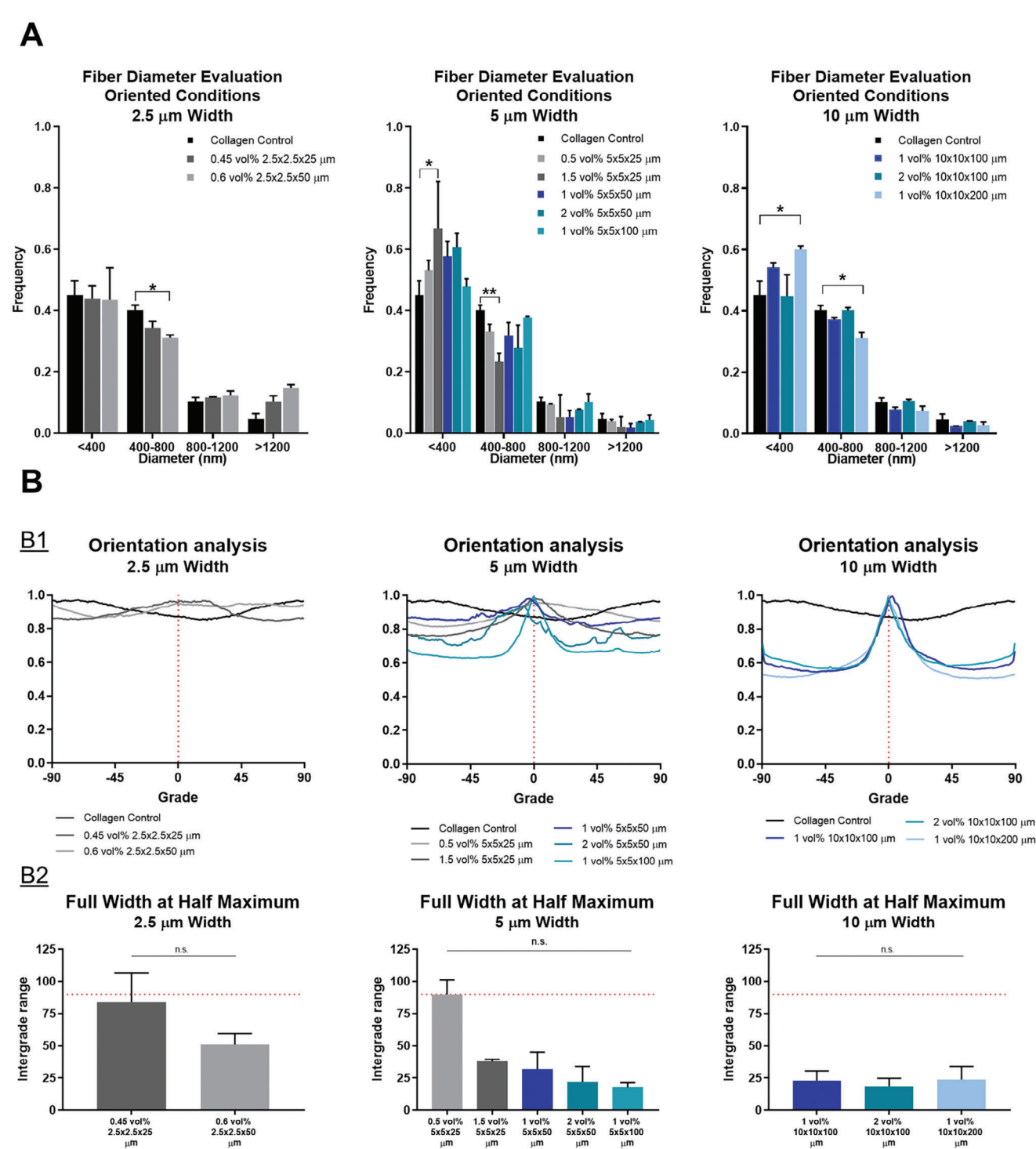


Figure 4. Collagen fiber characterization under oriented conditions. A) Diameter analysis regarding microgel cross-section. Data presented using bar graphs. with median and interquartile range. Kruskal–Wallis followed by Dunn's comparisons test was performed, *p < 0.05; **p < 0.01. B) Orientation analysis. B1) Orientation characterization of collagen fibers compared to microgel alignment. B2) Full Width at Half Maximum evaluation. Data presented using bar graphs. with median and interquartile range.

www.advancedsciencenews.com



www.advmattechnol.de

2.4. Collagen Fiber Orientation Analysis in Collagen-Anisogels

The Anisogel strategy has been extensively studied and characterized regarding microgel dimensions and aspect ratio.[30,40] In collagen-Anisogels, collagen fiber orientation was evaluated, using CRM images analyzed with Orientation I, an established Fiji plug-in. Figure 4B1 shows the orientation curves, from -90 to 90° for each width group and collagen control, with the direction of microgel orientation normalized to 0°. CRM images showed partial collagen fiber orientation along the magnetic field inside the collagen-Anisogel for all microgel sizes. To evaluate the differences between the partial alignments in each collagen-Anisogel and compare it to the random fiber orientation of the collagen control, we conducted an isolated analysis of FWHM between the maximum and minimum values for each condition (Figure 4B2). Among the partially oriented collagen fibers, the microgels with a larger width (10 µm) showed the highest collagen fiber orientation, with the small FWHM values (mean ranging from 18.67 to 23.75°) and no significant differences between the different lengths were observed. The broad distribution was achieved with the 2.5 µm wide microgels exhibiting high FWHM, while 5 µm wide microgels at 0.5 vol.% $5 \times 5 \times 25$ µm microgel condition showed a higher FWHM (90 \pm 11.3°) however no statistical differences were observed among conditions with longer or higher density of microgels formulations, as also seen in Figure 4B1. Interestingly, considering 5 µm wide microgels, specifically with a 25 or 50 µm length, we observed a decreasing FWHM, therefore an increase in fiber orientation, when the concentration of microgels is increased. These results were consistent with previous studies conducted by our group showing higher cell orientation in Anisogel conditions with higher concentrations of microgels.[31] Yet, such tendency was not observed in the case of larger microgels (10 \times 10 \times 100 μ m, at 1% and 2%) inside collagen-Anisogels, as both microgel concentrations showed low FWHM values.

Comparing different microgels widths, results revealed that an increase in collagen fiber orientation, characterized by a smaller FWHM was achieved with larger microgels with a width of $10\,\mu m$ and lengths equal or larger than $100\,\mu m$. This partial alignment of the collagen fibers will act together with the oriented PEG microgels to provide anisotropy to the collagen-Anisogels. Nevertheless, caution should be taken as a full fiber orientation was never achieved and discussion can only be done regarding partial orientation.

2.5. Normal Human Dermal Fibroblasts Cell Behavior in Collagen-Anisogels

Considering the results obtained so far, we performed cell in vitro studies with three types of collagen-Anisogels, using the conditions of: 0.6 vol.% 2.5 \times 2.5 \times 50 μm (no collagen fiber orientation), 1 vol.% 5 \times 5 \times 50 μm (intermediate partial collagen fiber orientation) and 2 vol.% 10 \times 10 \times 100 μm (high partial collagen fiber orientation). Figure S2 (Supporting Information) illustrates the control evaluation for collagen fiber orientation in collagen gels containing random microgels that were not magnetically aligned in the specified conditions, demonstrating no collagen alignment. Normal human dermal fibroblasts (NHDF)

were employed, as they are majorly producing and inhabiting in collagenous tissue.^[41] Cells were encapsulated in these formulations and cultured for 7 days. Collagen-Anisogels were analyzed for culture periods of 1, 5, and 7 days.

At each time point, cell orientation was measured by staining the actin filaments in all samples. On visual inspection, the actin micrographs (Figure 5A) showed cell orientation already from day 1 for all the three collagen-Anisogels conditions, as seen by the orientation distributions of the stained cytoskeleton (F-actin) (Figure 5B,C) and subsequent FWHM analysis (Figure 5D). A clear distinction of cell orientation was observed between the aligned collagen-Anisogels and collagen gels containing non-aligned microgels for each condition after 1 day of culture, as shown in Figure \$3 (Supporting Information). At day 1, all collagen-Anisogels conditions showed significant reduced FWHM values compared to collagen control (****p < 0.0001). Moreover, collagen-Anisogel condition using $10 \times 10 \times 100 \mu m$ microgels appeared to induce a higher cell orientation compared to smaller microgels (2.5 \times 2.5 \times 50 μ m, p = 0.0869). With time in culture (Figure 5D1), the $10 \times 10 \times 100$ µm collagen-Anisogels demonstrated consistency in providing cell anisotropy, always showing significant differences to cells encapsulated in collagen control regarding FWHM values (at day 1, ****p < 0.0001; at day 5, *p < 0.05; at day 7, **p < 0.01). 2.5 × 2.5 × 50 µm collagen-Anisogels exhibited significant higher cell orientation compared to collagen control (characterized by a reduced FWHM) only for day 1 and day 7 (****p < 0.0001; and *p < 0.05, respectively). Although $5 \times 5 \times 50 \,\mu m$ collagen-Anisogels showed significant alignment at day 1 compared to collagen control, this was not consistent with time in culture. Cell orientation results are according to the orientation of the collagen fibers inside these collagen-Anisogels (Figure 4B). When analyzing the behavior of the cells in each collagen-Anisogel throughout time (Figure 5D2), we observed a tendency for an increase of FWHM values with time, and therefore a reduction in cell orientation. This increase was more significant in $10 \times 10 \times 100$ µm collagen-Anisogels (day 1 versus day 5, p = 0.063; day 5 vs day 7, **p < 0.01) and may be due to the increased number of cells over time, which influences the cell material interaction causing strain-induced stiffening in collagen-Anisogels. Moreover, cells sense collagen substrate topography^[42] through mechanical forces and ECM interactions, which might be influencing the cells' ability to maintain their anisotropy. Further studies addressing the influence of cell proliferation on their orientation and its mechanobiological implication on collagen ECM should be conducted. Nevertheless, for 2 vol.% $10 \times 10 \times 100$ µm, cell orientation remained more aligned than in the control collagen gel throughout the period of culture, exhibiting the most favorable conditions for establishing a stable long-term anisotropy in collagen-Anisogels (Figure 5B-D).

Fibroblasts have been previously reported to align in anisotropic conditions. [43,44] Efficient cell adhesion and proliferation has been reported in a collagen/PEG hydrogel using human fibroblasts. [45] Similarly, our results demonstrated that NHDF cells efficiently grew within collagen-Anisogels, exhibiting alignment with the unidirectional orientation of the PEG microgels established during the initial gelation process and up to 7 days in culture. Mimicking native cell anisotropy is a key aspect for accurate design of in vitro models that recapitulate

2365709x, 2024, 8, Downloaded from https://onlinelibrary.wiley.com/doi/10.1002/admt.202301391 by Rwth Aachen Hochschulbibliothek, Wiley Online Library on [02.08/2024]. See the Terms and Conditions (https://onlinelibrary.wiley.com/doi/10.1002/admt.202301391 by Rwth Aachen Hochschulbibliothek, Wiley Online Library on [02.08/2024]. See the Terms and Conditions (https://onlinelibrary.wiley.com/doi/10.1002/admt.202301391 by Rwth Aachen Hochschulbibliothek, Wiley Online Library on [02.08/2024]. See the Terms and Conditions (https://onlinelibrary.wiley.com/doi/10.1002/admt.202301391 by Rwth Aachen Hochschulbibliothek, Wiley Online Library.

ions) on Wiley Online Library for rules of use; OA articles are governed by the applicable Creative Commons License

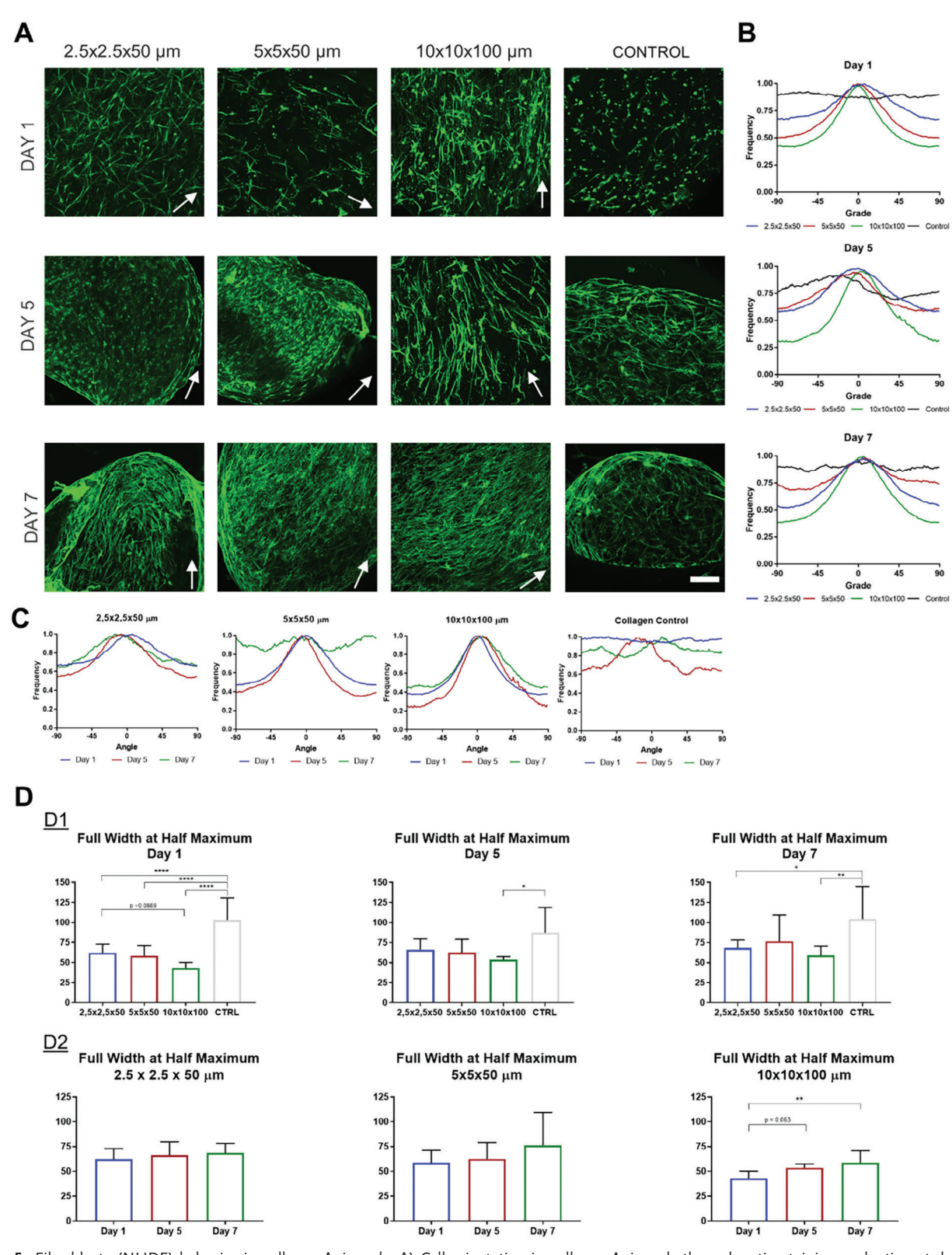


Figure 5. Fibroblasts (NHDF) behavior in collagen-Anisogels. A) Cell orientation in collagen-Anisogels through actin staining evaluation at day 1, 5, and 7. White arrows indicate the direction of the magnetic field and PEG microgels. Scale bar = $100 \,\mu\text{m}$. B) Actin orientation characterization per day in culture. C) Actin orientation characterization per microgel condition. D) Full Width at Half Maximum evaluation. Data presented using bar graphs. with mean and standard deviation. Ordinary one-way ANOVA followed by Tukey's multiple comparisons test was performed, p < 0.05, p < 0.01, p < 0.001.

nditions) on Wiley Online Library for rules of use; OA articles are governed by the applicable Creative Commons

SCIENCE NEWS

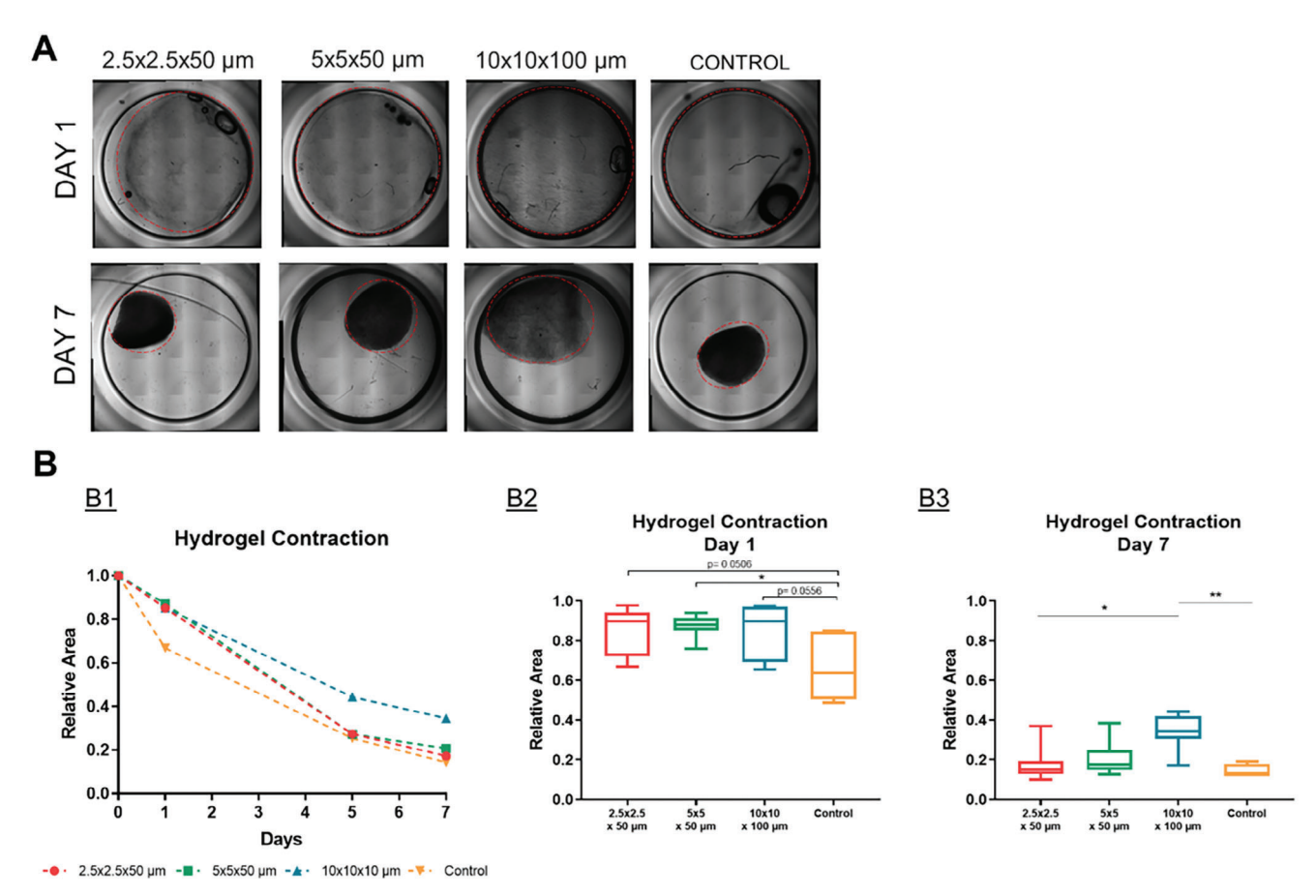


Figure 6. Cellular Hydrogels Analysis. A) Evaluation of hydrogel contraction. A1) Brightfield mosaic images of cellular hydrogels. B) Hydrogel contraction analysis by area evaluation (B1); Detailed comparison at day 1 (B2) and day 7 (B3). For B2, ordinary one-way ANOVA test was conducted, with Tukey's multiple comparison, p < 0.05. For B3, Kurskal–Wallis test was conducted, with Dunn's comparison, p < 0.05, p < 0.05.

tissue architecture and organization to resemble physiological conditions.^[46,47] In addition, these models are of interest to understand disease models in anisotropic collagenous tissues, which are sensitive to cellular forces and cell population, such as in musculoskeletal and cardiovascular research, allowing for a deeper understanding of the cellular alterations and for a better therapeutics design, among others.^[48,49]

2.6. Hydrogel Shrinkage Evaluation upon Cell Culture

The collagen hydrogels experienced shrinkage due to stress-induced matrix stiffening as expected in all hydrogels conditions. [50,51] This was observed visually at macroscopic level in **Figure 6A1**. To comprehend the effect of PEG-µgels in collagen-Anisogels, hydrogel contraction was evaluated by measuring the area revealing a reduction to near 20% at day 7 compared to day 0 (Figure 6B1). No macroscopical differences were observed when comparing shrinking between the collagen-Anisogels and collagen gels with random microgels (data not shown). At day 1 (Figure 6B2), the collagen control had a greater area reduction compared to collagen-Anisogels (*,p < 0.05 for 5 × 5 × 50 µm; p = 0.0506 for 2.5 × 2.5 × 50 µm; p = 0.0556 for 10 × 10 × 100 µm). At day 7 (Figure 6B3), there was a clear

reduction in hydrogel contraction in $10 \times 10 \times 100$ µm collagen-Anisogels compared to all other conditions, especially compared to 2.5 × 2.5 × 50 µm (*, p < 0.05) and to collagen control (**, p < 0.01), revealing that this condition not only promoted long-term oriented cell growth, but also limited strain-induced collagen contraction, which is often one of the key problems in collagen-based biomaterials development. [52,53]

An improvement of the shrinkage process has also been reported in a Col I hydrogel combined with PEG as a crosslinker, for skin applications,^[54] however in our case the PEG microgels were likely not covalently linked to the collagen. Tuning collagen hydrogel shrinkage is of paramount importance for a better development of in vitro models and implantable biomaterials, regarding cell culture time and therapeutic potential.^[53] Indeed, depending on the specific application, research has focused on both restrain shrinkage, as in for muscle tissue engineering,^[55] and in increasing shrinkage, to develop denser tissues and better resemble heart tissue.^[56]

Collagen-Anisogels have shown not only to induce collagen fiber orientation without impairing their mechanical properties, but also demonstrated the potential of in vitro collagen-based anisotropic models, allowing oriented cell growth and sustaining celullar orientation for several days. In collagen-Anisogels with larger microgels ($10 \times 10 \times 100 \ \mu m$), low hydrogel shrinkage was

www.advancedsciencenews.com

ADVANCED MATERIALS

www.advmattechnol.de

also observed, while for smaller size microgels $(2.5 \times 2.5 \times 50 \, \mu m)$ and for $5 \times 5 \times 50 \, \mu m)$ profound shrinkage was present, leading to opportunities for controlled collagen scaffold shrinkage using Anisogel-based models. This technology, therefore, shows promising opportunities in the bioengineering of in vitro functional tissues. Anisotropic formulations, here applied with Col I, are a key component of several organs in the human body, having well-established oriented structures in homeostatic conditions in several tissues, such as tendon, intervertebral disc, bone, among others. Therefore, the collagen-Anisogels developed here can be applied as a potential platform for different applications in tissue engineering, ultimately contributing to a better comprehension of anisotropic-related patho-mechanisms.

3. Conclusion

To our knowledge, this is the first study reporting an Anisogel composed by PEG rod-shaped microgels and Col I as surrounding gel. Besides evaluating the orientation properties of the hydrogel, we started by evaluating the impact on the collagen fibril when adding PEG microgels. Here, we demonstrated the maintenance of the key characteristics of collagen hydrogels considering fiber formation and mechanical properties. Moreover, we explored different dimensions and concentrations of PEG microgels to induce anisotropy by magnetically aligning the microgels during collagen gelation and studied the effect of this alignment on collagen fiber diameter and orientation. Microgels with larger width and length showed promising results in regulating collagen fiber orientation, without impairing fiber thickness. Human fibroblasts oriented along the microgels and collagen fibers, especially for the larger microgels, which also led to a reduction in hydrogel contraction, serving as a promising feature for further experiments. Future studies will include deeper analysis on other cell types and tissues, to recapitulate in vivo mechanisms and diseases and reassuring the potential of collagen-Anisogels as a platform for anistropic studies.

4. Experimental Section

Production of PEG Microgels: PEG microgels were prepared as previously described.[31] Briefly, microgels were produced by an in-mold polymerization method. The mold was prepared by mixing polydimethylsiloxane (PDMS, Sylgard 184, Dow Corning) with a thermo initiator (10:1 ratio), followed by pouring the mixed solution on silicon wafers (AMO GmbH) with different size patterns. The wafer with the liquid PDMS solution was cured at 110 °C for 4 h, while the PDMS mold was peeled off the wafer after curing. Next, a prepolymer solution (20 wt.% PEG di-acrylate (PEG-DA, Sigma Aldrich) and photoinitiator (Irgacure 2959, Sigma Aldrich) upon sonication was diluted in 200 Da PEG-OH (Sigma Aldrich) with 400 μg mL-1 SPIONs (EMG-700, Ferrotec)). The solution was poured on top of the PDMS mold and laminated with a polyethylene terephthalate (PET) foil (Goodfellow). By delaminating the PET film slowly, excess prepolymer solution was removed. The mold with PEG-DA solution was then cured in a nitrogen atmosphere for 60 min under UV light. Subsequently, the molds were cut in smaller sizes and glued on glass slides using a 50% polyvinylpyrrolidone glue (360 kDa, Sigma-Aldrich) layer, allowing the harvesting of the dried microgels by peeling the mold after 5 days at 37 °C. Microgels were harvested by dissolving the dried glue in water, purified multiple times in water by centrifugation, UV-sterilized, and disinfected in 70% ethanol. Last, microgels were washed in PBS (Lonza), quantified using a Neubauer chamber, and stored for a maximum of 4 weeks at 4 °C.

Production of Collagen-Anisogels: Type I collagen (Bovine skin, Sigma-Aldrich) working solutions were prepared following the manufacturer's instructions. Briefly, to achieve a $0.32\,\text{w/v}\%$ concentration, eight parts of collagen G (Sigma-Aldrich) were mixed with one part of Dulbecco's modified Eagle medium (DMEM) and one part of deionized water. The final solution was neutralized by adding $2\,\text{v/v}\%$ NaOH ($1\,\text{m}$). When PEG microgels were mixed within the collagen solution, the microgels were part of the one part of deionized water, without altering the final collagen concentration and maintaining the neutralization step. Different dimensions and concentrations of PEG microgels were used leading to several collagen-Anisogels formulations, as described in Figure 1B.

Analysis of Fibrillogenesis for Different Collagen-Anisogels Formulations: The polymerization kinetics of collagen-Anisogels formulations were measured through a turbidimetric assay. The described collagen-Anisogels solutions were prepared and neutralized as previously described and transferred to 96-well plates (glass bottom, Corning), which were previously cooled to 4 °C to inhibit an early onset gelation. Plates were loaded into a microplate reader (BioTek Synergy HT), which was pre-heated to 37 °C. Absorbance at 405 nm was measured for 2 h, at 30 s intervals. Kinetic parameters were calculated from the sigmoidal-shaped curves, which included lag time and maximum absorbance value.

Analysis of the Rheological Properties of Collagen-Anisogels Formulations: All collagen-Anisogels formulations were prepared as described in 2.2 and kept on ice prior to rheological measurements. A rheometer (TA instruments, DHR) with a cone-plate geometry (20 mm, 2.0°) was used. Time sweep analyses were conducted at 37 °C for 45 min for all tested formulations, after which a frequency (0.25–1 Hz) and amplitude (0.15–1%) sweep were performed, without magnetic stimulation, to confirm that the formulations were in the linear viscoelastic regime at the used conditions described in Table S1 (Supporting Information).

Preparation of Magnetically Oriented Collagen-Anisogels: Collagen-Anisogels formulations were prepared as described in 4.2. and kept on ice until casting on the ibidi chambers. Samples were casted in volumes between 10–20 μL in a well plate, in the presence of a uniform magnetic field of ≈ 100 mT, applied by using a pair of neodymium rectangle magnets (Magnosphere, Germany) (Figure 1A). Samples were incubated at RT for 5 min to allow for the orientation of the microgels within the hydrogels, and then transferred to an incubator at 37 °C for 60 min to trigger and complete the crosslinking of the collagen fibrils. Fresh media / PBS was added after the complete hydrogel crosslinking.

Analysis of Collagen Fibers: Collagen-Anisogels were produced as described in 4.2, together with control samples (not subjected to magnetic field), and stored in phosphate buffer saline (PBS 1x, pH 7.4). Confocal reflection microscopy (CRM) was used to acquire high-resolution images of the collagen fibers at high magnification (63x) in their native and hydrated state. Confocal imaging was performed using an SP8 Tandem Confocal (Leica Microsystems Inc.), with an argon-ion laser adjusted to 488 nm emission as a light source, used in reflection mode with a 63x oil immersion objective. Images were collected at 8-12 positions within three independent hydrogels per each different collagen-Anisogel. The 3D fiber network was evaluated considering fiber diameter and orientation, both quantified from images with Python and Fiji (free software (v2.0.0)) software, respectively. The reflection of PEG-µgels in the samples were removed prior to analysis (Figure 1C). Diameter analysis was written in python (https://www.python.org) using the libraries: numpy (https://numpy.org), matplotlib (https://matplotlib.org) and ImageP and BatchAnalyzer libraries developed by team, both available at github under https://www.github.com/tomio13/ImageP and https://www.github.com/ tomio13/BatchAnalyzer. Images were first blurred through convolution with a Gaussian kernel (standard deviation of 100 pixels, window size 801 pixels). This blurred image was subtracted as background, resulted negative values set to zero. Then the image was smoothed using another Gaussian kernel with standard deviation of 1 pixel, window size 11 pixels. For increasing the detail content, the dynamic range of the image was compressed setting the intensity values to a power of 0.5. Fibers were detected then applying a dynamic threshold calculated with the method of Otsu.[57] The width of the fibers were established employing a distance transform on the binary images (based on the work of [58]). Then a local

ADVANCED SCIENCE NEWS

www.advancedsciencenews.com

www.advmattechnol.de

maxima search was applied to collect the center points indicating the local radii of the fibers. The diameter values calculated from these local radii were then used to calculate a thickness histogram for each images. OrientationJ, a Java plugin for Fiji, [59] was used to map the directionality in the images (gradient: Gaussian; local window: 2 pixel), where each color is assigned to an orientation angle (Figure 1C).

Cell Encapsulation and 3D Cell Culture in Collagen-Anisogels: Normal human dermal fibroblasts (NHDF) (Promocell) were cultured in Dulbecco's modified Eagle's medium (DMEM; Gibco) supplemented with 10% FBS (Gibco) and 1% penicillin/streptomycin (Gibco) at 37 °C under 5% CO2. Cells from passages below 10 were used for the in vitro experiments. Briefly, collagen-Anisogels were prepared as described in section preparation of magnetically oriented collagen-anisogels, with cells being part of the eight-part collagen prior to mixing the other components. The casting of the precursor solutions in the presence of a uniform magnetic field was performed as above mentioned. Collagen-Anisogels with NHDF, and collagen hydrogels with NHDF as control, were kept in culture for 7 days, and culture media was replaced on day 5. Brightfield mosaic images with magnification of 10x were captured for each collagen gel at time day 1, 5, and 7 days of culture, using the confocal microscope. The hydrogel contraction was evaluated by area measurements using Fiji software.

Immunofluorescence Staining and Imaging: Hydrogels were fixed in 4% paraformaldehyde (PFA, AppliChem) in PBS for 40 min after 1, 5, and 7 days of culture. The samples were washed twice with PBS, permeabilized using 0.1% Triton X-100 (Sigma–Aldrich) in PBS for 40 min and washed twice again with PBS. Actin staining was performed by incubating the samples with phalloidin-iFluor 488 and 555 (1: 1000, Abcam) for 3 h, followed by PBS wash (2x) for 30 min. All samples were incubated during staining and washing steps in an elliptical plate shaker at 30 rpm. Samples were stored in PBS at 4 °C until imaging.

Z stack images of collagen-Anisogels with encapsulated cells were imaged using a 10x magnification air objective in a laser scanning confocal microscope (SP8 Tandem Confocal, Leica Microsystems Inc). The light source used was an argon-ion laser adjusted to 488 and 555 nm emission (fluorescence from microelements). Z-stack images were collected from 2–3 random locations in the middle of the hydrogels, with a stack size between 50 and 150 μm for the three biologically relevant replicas for each independent time point (1, 5, and 7 days of culture). Actin orientation was quantified by superimposing the z-stack images, using Fiji software. Cell orientation was evaluated following the same procedure described before for fiber orientation analysis.

Statistical Analysis: Statistical analysis was performed using GraphPad Prism software (v5). A Shapiro Wilk normality test was used to assess data normality. When a normal distribution was verified, one-way ANOVA analysis followed by Tukey's multiple comparison test was performed, and results were presented using mean and standard deviation. For analysis not following a normal distribution, a Kruskal–Wallis test followed by corrected Dunn's were performed, and results were presented using median and interquartile range. For evaluations regarding paired experiments, upon normality assessment, Friedman test followed by Dunn's comparison were conducted. Statistical significance was considered for *p < 0.05; **p < 0.01; ****p < 0.001; ****p < 0.001.

Supporting Information

Supporting Information is available from the Wiley Online Library or from the author.

Acknowledgements

A.L.C. acknowledges Fundação para a Ciência e a Tecnologia (FCT) for the PhD Grant (SFRH/BD/147300/2019) and the International Doctoral Program in Molecular and Cellular Biotechnology applied to Health Sciences (BiotechHealth). S.V. and L.D.L. thanks the support from universities of excellence funding line (Grant no. EXS-PFLS010) RWTH, Aachen. A.L.C., R.M.G., and L.D.L. acknowledge FCT and the Deutscher Akademischer

Austauschdienst for the Programme for Cooperation in Science between Portugal and Germany (Grant no: 2021.09716.CBM)

Open access funding enabled and organized by Projekt DEAL.

Conflict of Interest

The authors declare no conflict of interest.

Author Contributions

M.A.B, R.M.G., and L.D.L. conceptualized and designed the idea for the study. A.L.C., S.V., and L.D.L. performed analysis and interpretation of the data. T.H. designed software for the study. A.L.C. and S.V. performed drafting of the article. M.A.B., R.M.G., and L.D.L. performed critical revision of the article for important intellectual content and final approval. M.A.B., R.M.G., and L.D.L. performed supervision. R.M.G. and L.D.L. performed funding acquisition. All authors have read and agreed to the published version of the manuscript.

Data Availability Statement

The data that support the findings of this study are available from the corresponding author upon reasonable request.

Keywords

anisotropy, collagen type I, in vitro models, magnetic microgels

Received: August 24, 2023 Revised: December 24, 2023 Published online: February 15, 2024

- P., Fratzl, in Collagen: Structure and Mechanics, Springer US, Boston, MA, 2008, pp. 1–13.
- [2] J. Glowacki, S. Mizuno, Biopolymers 2008, 89, 338.
- [3] C. H. Lee, A. Singla, Y. Lee, Int. J. Pharm. 2001, 221, 1.
- [4] D. J. Hulmes, J. Struct. Biol. 2002, 137, 2.
- [5] A. K. Lynn, I. V. Yannas, W. Bonfield, J. Biomed. Mater. Res. B Appl. Biomater. 2004, 71, 343.
- [6] Y. H. Chun, S.-K. Park, E. J. Kim, H. J. Lee, H. Kim, W.-G. Koh, G. F. Cunha, D. Myung, K.-S. Na, Sci. Rep. 2021, 11, 23913.
- [7] P. Zhang, L. Xu, J. Gao, G. Xu, Y. Song, G. Li, J. Ren, Y. Zhang, C. Yang, Y. Zhang, R. Xie, N. Zhang, H. Yang, Bioact. Mater. 2022, 10, 255.
- [8] S. Rother, G. Ruiz-Gómez, K. Balamurugan, L. Koehler, K. M. Fiebig, V. D. Galiazzo, U. Hempel, S. Moeller, M. Schnabelrauch, J. Waltenberger, M. T. Pisabarro, D. Scharnweber, V. Hintze, ACS Appl Bio Mater 2021, 4, 494.
- [9] A. Dewle, N. Pathak, P. Rakshasmare, A. Srivastava, ACS Biomater. Sci. Eng. 2020, 6, 779.
- [10] P. Datta, V. Vyas, S. Dhara, A. R. Chowdhury, A. Barui, J. Bionic Eng. 2019, 16, 842.
- [11] L. A. Hapach, J. A. VanderBurgh, J. P. Miller, Phys. Biol. 2015, 12, 61002.
- [12] A. Ahmed, I. M. Joshi, M. Mansouri, N. N. N. Ahamed, M.-C. Hsu, T. R. Gaborski, V. V. Abhyankar, Am. J. Physiol. Cell Physiol. 2021, 320, C1112.
- [13] Y. Wakuda, S. Nishimoto, S.-i Suye, S. Fujita, Sci. Rep. 2018, 8, 6248.
- [14] C. J. Lowe, I. M. Reucroft, M. C. Grota, D. I. Shreiber, ACS Biomater. Sci. Eng. 2016, 2, 643.

articles are governed by the applicable Creative Commons

www.advancedsciencenews.com www.advmattechnol.de

- [15] H. R. Hoogenkamp, G.-J. Bakker, L. Wolf, P. Suurs, B. Dunnewind, S. Barbut, P. Friedl, T. H. van Kuppevelt, W. F. Daamen, Acta Biomater. 2015. 12, 113.
- [16] H.-Y. Xu, N. Gu, Front. Mater. Sci. 2014, 8, 20.
- [17] J. A. Paten, S. M. Siadat, M. E. Susilo, E. N. Ismail, J. L. Stoner, J. P. Rothstein, J. W. Ruberti, ACS Nano 2016, 10, 5027.
- [18] B. S. Jha, C. E. Ayres, J. R. Bowman, T. A. Telemeco, S. A. Sell, G. L. Bowlin, D. G. Simpson, J. Nanomater. 2011, 2011, 348268.
- [19] M. P. Prabhakaran, E. Vatankhah, S. Ramakrishna, Biotechnol. Bioeng. 2013. 110. 2775.
- [20] K. S. Rho, L. Jeong, G. Lee, B.-M. Seo, Y. J. Park, S.-D. Hong, S. Roh, J. J. Cho, W. H. Park, B.-M. Min, *Biomaterials* 2006, 27, 1452.
- [21] J. X. Law, L. L. Liau, A. Saim, Y. Yang, R. Idrus, Tissue Eng. Regen. Med. 2017, 14, 699.
- [22] D. I. Zeugolis, S. T. Khew, E. S. Y. Yew, A. K. Ekaputra, Y. W. Tong, L.-Y. L. Yung, D. W. Hutmacher, C. Sheppard, M. Raghunath, *Biomaterials* 2008, 29, 2293.
- [23] R. Ozasa, A. Matsugaki, Y. Isobe, T. Saku, H.-S. Yun, T. Nakano, J. Biomed. Mater. Res., Part A 2018, 106, 360.
- [24] S. Yang, X. Shi, X. Li, J. Wang, Y. Wang, Y. Luo, Biomaterials 2019, 207, 61.
- [25] M. Antman-Passig, O. Shefi, Nano Lett. 2016, 16, 2567.
- [26] T. Novak, S. L. Voytik-Harbin, C. P. Neu, Acta Biomater. 2015, 11, 274.
- [27] A. Miri, H. Najafzadeh, M. Darroudi, M. J. Miri, M. A. J. Kouhbanani, M. Sarani, Chemistry Open 2021, 10, 327.
- [28] J. C. Rose, D. B. Gehlen, T. Haraszti, J. Köhler, C. J. Licht, L. De Laporte, Biomaterials 2018, 163, 128.
- [29] J. C. Rose, M. Cámara-Torres, K. Rahimi, J. Köhler, M. Möller, L. De Laporte, Nano Lett. 2017, 17, 3782.
- [30] J. C. Rose, D. B. Gehlen, A. Omidinia-Anarkoli, M. Fölster, T. Haraszti, E. E. Jaekel, L. De Laporte, Adv. Healthcare Mater. 2020, 9, e2000886
- [31] S. Babu, I. Chen, S. Vedaraman, J. Gerardo-Nava, C. Licht, Y. Kittel, et al., Adv. Funct. Mater. 2022, 32, 2202468.
- [32] S. Vedaraman, D. Bernhagen, T. Haraszti, C. Licht, A. Castro Nava, A. Omidinia Anarkoli, et al., *Biomater. Sci.* 2021, 9, 4329.
- [33] Y. Ran, W. Su, L. Ma, X. Wang, X. Li, Int. J. Biol. Macromol. 2021, 166, 1480
- [34] S. T. Kreger, B. J. Bell, J. Bailey, E. Stites, J. Kuske, B. Waisner, S. L. Voytik-Harbin, *Biopolymers* 2010, 93, 690.
- [35] D. M. Darvish, Mater Today Bio 2022, 15, 100322.
- [36] A. O. Brightman, B. P. Rajwa, J. E. Sturgis, M. E. McCallister, J. P. Robinson, S. L. Voytik-Harbin, *Biopolymers* 2000, 54, 222.
- [37] Y. L. Yang, C. Sun, M. E. Wilhelm, L. J. Fox, J. Zhu, L. J. Kaufman, Biomaterials 2011, 32, 7932.
- [38] C. A. Bashur, L. A. Dahlgren, A. S. Goldstein, *Biomaterials* 2006, 27, 5681.

- [39] H. C. Hsia, M. R. Nair, R. C. Mintz, S. A. Corbett, *Plast. Reconstr. Surg.* 2011, 127, 2312.
- [40] J. C. Rose, M. Fölster, L. Kivilip, J. L. Gerardo-Nava, E. E. Jaekel, D. B. Gehlen, W. Rohlfs, L. De Laporte, *Polym. Chem.* 2020, 11, 496.
- [41] V. S. LeBleu, E. G. Neilson, FASEB J. 2020, 34, 3519.
- [42] A. Dede Eren, E. D. Eren, T. J. S. Wilting, J. de Boer, H. Gelderblom, J. Foolen, Sci. Rep. 2021, 11, 1516.
- [43] S. Wang, D. P. Maruri, J. M. Boothby, X. Lu, L. K. Rivera-Tarazona, V. D. Varner, T. H. Ware, J. Mater. Chem. B 2020, 8, 6988.
- [44] S. Konar, P. Edwina, V. Ramanujam, A. Arunachalakasi, S. K. Bajpai, J. Biomed. Mater. Res. B Appl. Biomater. 2020, 108, 2368.
- [45] B. K. Chan, C. C. Wippich, C. J. Wu, P. M. Sivasankar, G. Schmidt, Macromol. Biosci. 2012, 12, 1490.
- [46] J. L. Gerardo-Nava, J. Jansen, D. Günther, L. Klasen, A. L. Thiebes, B. Niessing, C. Bergerbit, A. A. Meyer, J. Linkhorst, M. Barth, P. Akhyari, J. Stingl, S. Nagel, T. Stiehl, A. Lampert, R. Leube, M. Wessling, F. Santoro, S. Ingebrandt, S. Jockenhoevel, A. Herrmann, H. Fischer, W. Wagner, R. H. Schmitt, F. Kiessling, R. Kramann, L. De Laporte, Adv. Healthcare Mater. 2023, 12, 2301030.
- [47] A. Mathur, Z. Ma, P. Loskill, S. Jeeawoody, K. E. Healy, Adv. Drug Delivery Rev. 2016, 96, 203.
- [48] S. Caddeo, M. Boffito, S. Sartori, Front. Bioeng. Biotechnol. 2017, 5, 40.
- [49] M. Gomez-Florit, C. J. Labrador-Rached, R. M. A. Domingues, M. E. Gomes, Adv. Drug Delivery Rev. 2022, 185, 114299.
- [50] M. Bacakova, J. Pajorova, A. Broz, D. Hadraba, F. Lopot, A. Zavadakova, L. Vistejnova, M. Beno, I. Kostic, V. Jencova, L. Bacakova, Int. J. Nanomed. 2019, 14, 5033.
- [51] C. Helary, I. Bataille, A. Abed, C. Illoul, A. Anglo, L. Louedec, D. Letourneur, A. Meddahi-Pellé, M. M. Giraud-Guille, *Biomaterials* 2010, 31, 481.
- [52] E. Bell, B. Ivarsson, C. Merrill, Proc. Natl. Acad. Sci. USA 1979, 76, 1274
- [53] S. O. Sarrigiannidis, J. M. Rey, O. Dobre, C. González-García, M. J. Dalby, M. Salmeron-Sanchez, Mater. Today Bio. 2021, 10, 100098.
- [54] C. Lotz, F. F. Schmid, E. Oechsle, M. G. Monaghan, H. Walles, F. Groeber-Becker, ACS Appl. Mater. Interfaces 2017, 9, 20417.
- [55] J. Foolen, V. S. Deshpande, F. M. W. Kanters, F. P. T. Baaijens, *Biomaterials* 2012, 33, 7508.
- [56] W. H. Zimmermann, I. Melnychenko, G. Wasmeier, M. Didié, H. Naito, U. Nixdorff, A. Hess, L. Budinsky, K. Brune, B. Michaelis, S. Dhein, A. Schwoerer, H. Ehmke, T. Eschenhagen, *Nat. Med.* 2006, 12, 452.
- [57] N. Otsu, IEEE Trans. Syst. Man Cybern. 1979, 9, 62.
- [58] P. F. Felzenszwalb, D. P. Huttenlocher, Theory Comput. 2012, 8, 415.
- [59] E. Fonck, G. G. Feigl, J. Fasel, D. Sage, M. Unser, D. A. Rüfenacht, N. Stergiopulos, Stroke 2009, 40, 2552.